Monte Carlo simulation of a protontherapy platform devoted to ocular melanoma

J. Hérault, N. Iborra, B. Serrano, and P. Chauvel

Articles you may be interested in

Calculated organ doses using Monte Carlo simulations in a reference male phantom undergoing HDR brachytherapy applied to localized prostate carcinoma
Med. Phys. **40**, 033901 (2013); 10.1118/1.4791647

Monte Carlo simulation of contrast-enhanced whole brain radiotherapy on a CT scanner
Med. Phys. **38**, 4672 (2011); 10.1118/1.3609099

GPUMCD: A new GPU-oriented Monte Carlo dose calculation platform
Med. Phys. **38**, 754 (2011); 10.1118/1.3539725

Monte Carlo simulation estimates of neutron doses to critical organs of a patient undergoing 18 MV x-ray LINAC-based radiotherapy
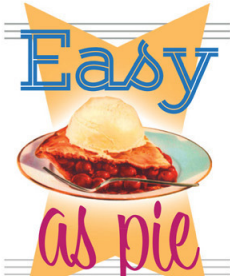Med. Phys. **32**, 3579 (2005); 10.1118/1.2122547

Magnetic confinement of electron and photon radiotherapy dose: A Monte Carlo simulation with a nonuniform longitudinal magnetic field
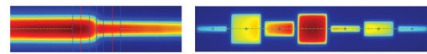Med. Phys. **32**, 3810 (2005); 10.1118/1.2011091

Monte Carlo simulation of a protontherapy platform devoted to ocular melanoma

J. Hérault[a)] and N. Iborra
Centre Antoine Lacassagne, Cyclotron Biomédical, 227 Avenue de la Lanterne, 06200 Nice, France

B. Serrano
Laboratoire de Physique Electronique des Solides, LPES-CRESA, EA 1174, Université de Nice Sophia-Antipolis, Parc Valrose, 06108 Nice Cedex 2, France

P. Chauvel
Centre Antoine Lacassagne, Cyclotron Biomédical, 227 Avenue de la Lanterne, 06200 Nice, France

Patients with ocular melanoma have been treated since June 1991 at the medical cyclotron of the Centre Antoine Lacassagne (CAL). Positions and sizes of the ocular nozzle elements were initially defined based on experimental work, taking as a pattern functional existing facilities. Nowadays Monte Carlo (MC) calculation offers a tool to refine this geometry by adjusting size and place of beam modeling devices. Moreover, the MC tool is a useful way to calculate the dose and to evaluate the impact of secondary particles in the field of radiotherapy or radiation protection. Both LINAC and cyclotron producing x rays, electrons, protons, and neutrons are available in CAL, which suggests choosing MCNPX for its particle versatility. As a first step, the existing installation was input in MCNPX to check its aptitude to reproduce experimentally measured depth-dose profile, lateral profile, output-factor (OF), and absolute dose. The geometry was defined precisely and described from the last achromatic bending magnet of our proton beam line to the position of treated eyes. Relative comparisons of percentage depth-dose and lateral profiles, performed between measured data and simulations, show an agreement of the order of 2% in dose and 0.1 mm in range accuracy. These comparisons, carried out with and without beam-modifying device, yield results compatible to the required precision in ocular melanoma treatments, as long as adequate choices are made on MCNPX input decks for physics card. Absolute dose and OF issued from calculations and measurements were also compared. Results obtained for these two kinds of data, carried out in the simplified situation of an unmodulated beam, indicate that MC calculation could effectively complement measurements. These encouraging results are a large source of motivation to promote further studies, first in a new design of the ocular nozzle, and second in the analysis of the influence of beam-modifying devices attached to the final patient collimator, such as wedge or compensators, on dose values. © *2005 American Association of Physicists in Medicine.*
[DOI: 10.1118/1.1871392]

Key words: Monte Carlo, MCNPX, ocular, proton, therapy

I. INTRODUCTION

The Nice hadrontherapy platform was the first site in France starting to treat patients with protons in June 1991. Up to now 2500 patients have been treated for eye melanoma, conjunctival melanoma, and angioma. A provisional set of clinical results was the subject of publications for the first 538 cases in 1999[1] and more recently in 2004[2,3] for patients coming from the region of Lyons (France).

The ocular proton beam line was initially conceived and built on the basis of experimental measurements of percentage depth dose and lateral dose profiles that allowed optimization of position, size, and number of collimators and diffusion devices. This initial preparation did not investigate all technical solutions; the Monte Carlo (MC) calculation could present an alternative to experimental measurements to improve beam quality parameters such as flatness or penumbra. MC is also a potential tool to explore absorbed dose and related processes, like energy loss, multiple Coulomb scattering (MCS), or secondary protons or neutrons production. A better knowledge of these processes is essential to complement experimental work where measurements are technically difficult to perform such as for too small collimator size. In these particular conditions, MC becomes a useful tool to extend information beyond the conditions where measurements are possible. In a wider context, the MC simulation could help experimental measurements, in the fields of radiotherapy and radiation protection. However, before using it in an extensive manner, the quality of its response must be checked with the existing measurement data.

The well-known MC code MCNP was recently extended to include protons in the MCNPX[4] version and appears as an ideal particle transport code which is valuable for all particles in our Centre, using cyclotron and LINAC machines for radiotherapy. The use of MC is widely documented for
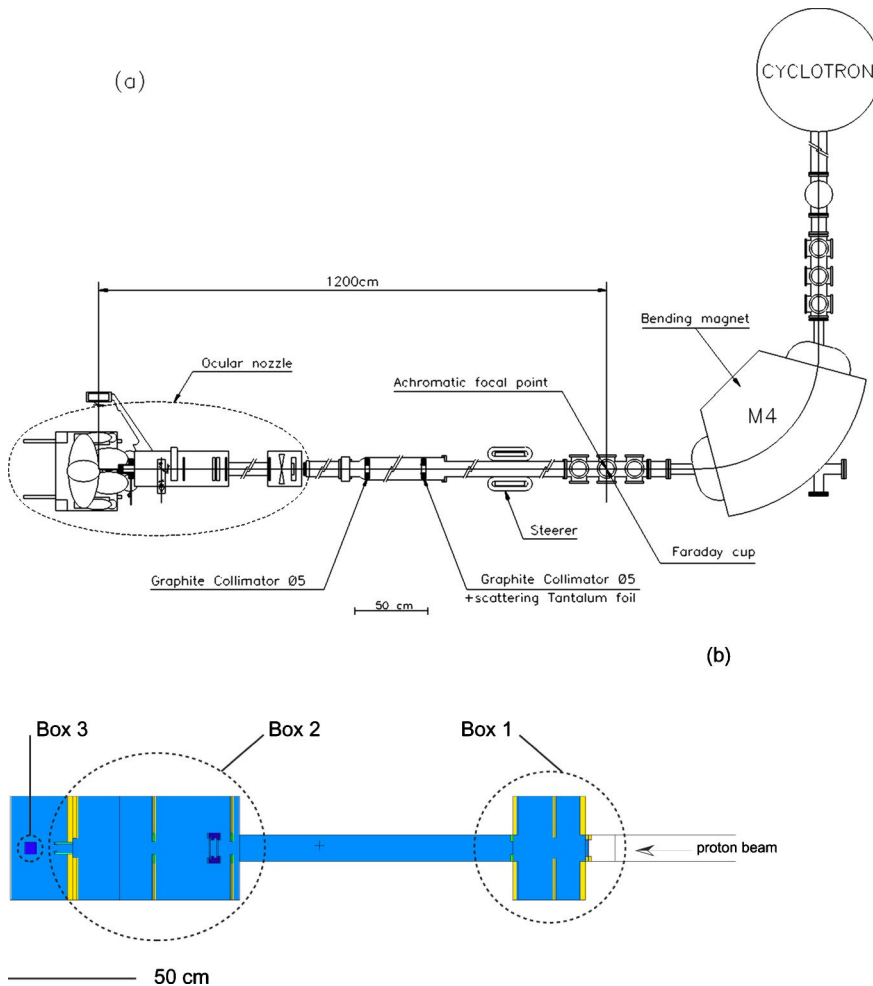
FIG. 1. (a) Ocular nozzle and proton beam line schema. The achromatic focal point of the bending magnet M4 corresponds to the proton source point described in MCNPX. Two graphite collimators are present in the vacuum pipe, with one of them supporting the tantalum foil scatter. The FC controls the incoming intensity of the proton beam. (b) Ocular nozzle setup as MCNPX viewed on a longitudinal section *xz*. Box 1 holds the Lucite propeller and range shifter, box 2 contains monitor chambers and reticules, and box 3 represents the water phantom.

LINAC,[5] but such type of information in the field of proton-therapy is scarcer.[6–8]

First, the absorbed dose in a water phantom set at the eye position of an incoming unmodulated proton beam was studied. Central-axis percentage depth-dose profiles and lateral dose profiles were simulated, measured, and then analyzed, in order to adapt the MCNPX physics model to experimental data. The energy spectrum was also calculated at the entrance of the water phantom to determine the energy extent of the proton population. At this same entrance, the absolute dose and its variation with collimator size were calculated and measured.

Second, calculations closer to a clinical situation were analyzed by adding a Lucite propeller to produce a spread-out Bragg peak (SOBP). Related central-axis percentage depth-dose profiles and lateral dose profiles were calculated and compared to experimental data.

With this set of comparisons between experimental and simulated data, this work aims to evaluate the potential and the quality of the MC tool, MCNPX, in the field of ocular protontherapy.

II. MATERIAL AND METHODS

A. Beam line configuration

The hospital-based cyclotron MEDICYC[9,10] provides 65 MeV protons. The accelerator is a fixed frequency 25 MHz isochronous cyclotron with a peak voltage of 50 kV. Negative hydrogen ions are produced by an external source, axially injected and accelerated to 65 MeV. They are then extracted by a 60×10^{-6} g cm^{-2} carbon stripping foil and exiting protons are transported down the beam line to the treatment room.

The main components of the ocular beam line are presented in Fig. 1(a). The incoming proton beam is completely defocused after the achromatic focal point of the last 90° bending magnet (M4), regarded as the source point for calculations, before reaching a 5×10^{-3}-cm-thick tantalum foil. These elements act together as a single scatterer providing 12 m behind away, a flat beam at the irradiation point. In the vacuum part, upstream from the ocular nozzle, the beam aperture is limited to 5 cm diameter by two graphite collimators. Afterwards, decreasing the collimator size from 5 to 4.5 and finally 3.4 cm, only the central part of the beam is selected. The ocular nozzle part of the beam line is described as a MCNPX geometry plot in Fig. 1(b), on a longitudinal *xz* section. Box 1 is closed at its extremities by two brass collimators opened to a 5 cm diameter; a kapton foil 1.3 10^{-2} cm thick, sparing vacuum to air, also closes its upstream extremity. This empty box holds the range shifter and the Lucite propeller, which are used to adapt the incoming proton beam in range and modulation. Box 2 contains two monitor chambers made of aluminized mylar, two 4.5 cm

brass collimators, and an exiting copper nozzle of 3.4 cm internal diameter, which supports the final individual brass patient collimator. Box 3 is the water phantom simulating the eye irradiation.

In the clinical situation SOBP are required to provide homogeneous irradiation in depth, z. The corresponding depth-dose curve $D(z)$ is obtained by adding the weighted contribution of individual (i) reduced Bragg peak curves $D_i(z)$,[11] achieved by the introduction of a thickness of Lucite t,

$$D(z) = \sum_{i=0}^{n} p_i D_i(z),$$

$$t = ns,$$

where p_i represents the weighting factor of the reduced peak i, n is the total number of peaks needed to achieve a defined length of SOBP t, z is the depth of irradiation, and s is the thickness step of reducing material equal to 8×10^{-2} cm.

B. Experimental beam diagnostics

Three sorts of beam diagnostics were used to check the accuracy of the MC calculation; small silicon diode (SD), ionization chambers (IC), and Faraday cup (FC).

Beam profiles were measured in transverse direction by using an automated scan system, which moves a small and thin commercial SD in a small water tank ($13 \times 10 \times 6$ cm^3). The silicon sensitive area is ($10^{-1} \times 3 \ 10^{-1} \times 10^{-2}$ cm^3), allowing very small beam sizes to be accurately measured, even in a high gradient dose region. Dimensions of the water phantom are well adapted to small field size measurements typical of the eye melanoma irradiation. By nature the water is representative of the eye tissue, with a density close to the mean eye one ($\rho = 1.05$ g cm^{-3}).

Percentage depth dose profiles were measured using an Exradin T11 parallel plate IC. The corresponding measurements were carried out for discrete steps, as no remote control was available for displacements.

Absolute absorbed dose determinations were performed with Exradin T1 thimble IC presenting a $5 \ 10^{-2}$ cm^3 detection volume, applying the European code of practice for clinical dosimetry.[12,13] A homemade FC[14] was also used for fluence measurements and absolute dosimetric determination. Commercial FCs, carbon made, were also employed to measure and control the beam current all along the beam line.

C. MCNPX code

MCNPX is a general purpose Monte Carlo style program for radiation problem. For proton transport up to 150 MeV, it uses at choice the cross sections library LA150H or physics models (PM) to calculate interaction probabilities. These models are taken from other codes included in MCNPX, notably the LAHET[15] Code System (LCS) containing the Bertini and ISABEL models. Between nuclear interactions, particle tracking involves atomic electron interactions that cause a charged particle to lose energy along its track length. The

proposed collision energy-loss model leads to stopping powers in a closer ICRU[16] compliance, except for the low energy range where 7% and 3% higher values were, respectively, found for 1 and 2 MeV energies. The energy loss straggling is implemented and described producing improved results in range calculations when selected. A variable of physics card controls selection of straggling model based on the Vavilov[17] theory. When the variable is not amended, calculations are performed in the continuous slowing down approximation (CSDA). The MCS is also implemented and relies on Rossi's theory, assuming a Gaussian distribution of angular deflections. In MCNPX, neglecting the small spatial proton displacements makes an additional approximation. Contrary to energy-loss straggling, there is no free parameter to turn off MCS. Particles tracked were only protons and neutrons, as "delta rays" of knock-on electrons for charged heavy particles are not produced yet in MCNPX. Two methods are available to tally energy deposition. The first one is the F6 tally that scores dose on geometrical elements defined as part of the standard problem geometry. The second one is the energy deposition mesh tally type 3. This new mesh tally capability for MCNPX is currently in standard use in most high-energy Monte Carlo codes. The dose is scored on a rectangular, cylindrical, or spherical grid overlaid on top of the standard problem geometry. Energy cut-off was set to their minimal value, i.e., 1 MeV, and energy particles which fall below are deposited locally.

MCNPX (V2.4) was run with a PC under a Windows operating system. Depending on the complexity of the problem and the accuracy needed, the number of particles followed varies from 10^6 to 10^9 histories. Corresponding results were output in times ranging from hours to days, for a Pentium IV processor. No approximation was made for geometry description for objects on the beam trajectory; even small objects, like reticules defining the irradiation plane and composed by two tungsten wires of diameter 1.5×10^{-2} cm were described, to get a simulation closest to reality.

First, the water phantom was arranged as a lattice of small spheres filling it to score doses with a F6 tally. Second, it was arranged as an ensemble of cylindrical or rectangular meshes with variable sizes to calculate doses with mesh tally type 3. No difference is oberved between the two methods. As methods for dose calculation gave equivalent results, mesh 3 tally was used in further calculations, for its simplest geometry description and easiest analysis possibilities.

III. RESULTS AND DISCUSSION

A. Unmodulated beam

At the beginning, great importance was attached to describing a precise geometry. We first tested the beam alone without any beam-modifying device, to search for better physics options producing the most adherent simulated data to experimental values. The two available MCNPX beam physics options, invoking PM or LA150H library uses, were tested for proton transport.[4]

TABLE I. Proton yields intensity measured and simulated between water phantom and source and water phantom and box 1 entrance. Calculations were performed with MCNPX in LA150H library physics options.

Proton yield intensity	Water phantom/source	Water phantom/box 1 entrance
Measurements	1.2×10^{-2}	0.53
MCNPX	2.3×10^{-3}	0.52

1. Beam source

The raw beam source was described as 1 cm size, Gaussian distributed in space with a full width at half maximum (FWHM) at 0.75 cm, limited by a beam emittance set to 10 mrad. The energy was set to 65 MeV, Gaussian distributed with a FWHM at 0.130 MeV. These values were issued on the one hand from beam transport calculation and on the other hand from size observation with an interceptive method. The whole beam line was designed for beam optics with the TRANSPORT[18] program which provides a matrix relating the coordinates, angles and transverse momenta of the proton beam, giving at the focal point of the last bending magnet M4 an interesting information concerning beam emittance. This information is completed by measurements of beam spot on an alumina screen that is pneumatically inserted in the beam path. The achievement of beam source definition for its geometric components was not fully satisfying, as shown in Table I. There is a large difference in the ratio of beam intensities measured with FC and simulated with MC between the water phantom entrance and the source point. The calculated value was the division result of the number of proton tracks entering the water phantom by the number of protons emitted from source. The intensity transmission throughout the beam line essentially depends on beam source emittance definition and the thickness introduced on beam trajectory that deflects protons laterally. Beam emittance reduction alone was not sufficient enough to converge toward the expected experimental value, even if it was zeroed. As there is no free parameter to turn off MCS to study its influence, the tantalum foil scatter was adjusted to half of its thickness value to simulate a lower value of the mean scattered angle. In these conditions, beam intensity yield calculations and measurements agreed. These facts suggested that MCS description[19–22] in the MCNPX code was responsible for this failure, overestimating angular deflection. The scatter foil is a very thin layer of high Z material, two physical characteristics leading to smaller mean diffusion angle and appearance of large angle single scattering events. The appliance of the Gaussian Rossi's formula fails in these cases and must be replaced by a full Molière's theory implementation.[19–22] This deficiency was enlightened because beam source parameters were measured and not estimated as it was generally done. It was clearly perceptible because of the length of the proton beam line, roughly 12 m, which act as a telescope on the measurements. In these very sensible geometric conditions, an error of just a few mrad on mean scattered angle can cause such discrepancy on beam intensity yield. An additional series of beam intensity measurements was performed only in the air part of the proton beam line between the box 1 entrance and the water phantom. At this time, measurements were realized with an IC, as the available place in box 1 was too narrow to admit FC. These measurements for the last 2.2 m of the ocular nozzle are in accordance with the MC value (Table I). The experimental value derived from dose ratios demonstrates a correct proton beam intensity spread out for the beam line ending. This additional series indicates the deficiency of beam transmission on the scatter foil, sole element present on beam path in the vacuum beam line section. As beam intensity yield was not perturbed for the whole ocular nozzle by initial discrepancies observed in the vacuum beam line section, further dosimetric investigations can be performed. However, particular attention was maintained in normalization per initial source particle sense. A phase space containing 0.5×10^9 protons was created at the entrance of box 1 [Fig. 1(b)] to speed up subsequent calculations, since the beam line setup was frozen from proton source to this plane.

2. Energy spectrum

The energy spectrum at the entrance of the beam line was stated as Gaussian, distributed around 65 MeV with a FWHM of 0.130 MeV and corresponding roughly to one tour for protons on the cyclotron. The presence of the ocular

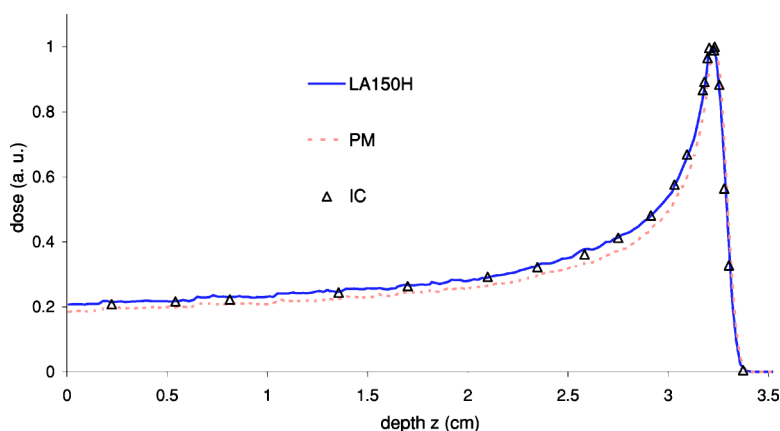FIG. 2. Relative absorbed dose to water, dose, as a function of water depth, z. Percentage depth-dose, calculated with MCNPX in PM (dashed line) and LA150H library (continuous line) physics options and measured with parallel plate IC (triangle) for a final collimator diameter size set to 2.5 cm. Calculation step size is 0.02 cm. MC type A and parallel plate IC type B uncertainties are, respectively, on the order of 0.5% and 4%.
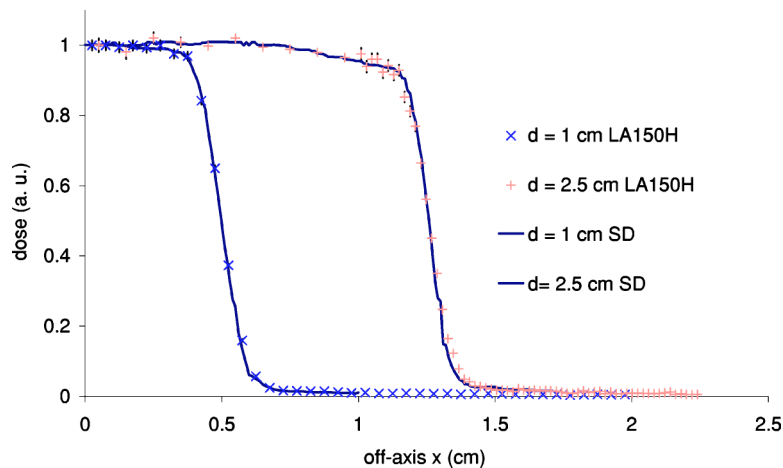
FIG. 3. Relative absorbed dose to water, dose, vs lateral position, *x*. Lateral dose profiles calculated with MCNPX in LA150H library physics option, for two final collimator diameter sizes set to 1.0 cm ($\times$) and 2.5 cm ($+$), at the entrance of the water phantom. Measurements performed with SD (continuous line) are also displayed. Calculation step size is irregular; its value is 0.02 cm in the penumbra. MC type A and SD type B uncertainties are, respectively, on the order of 0.5% and 4%.

nozzle elements such as tantalum scatter foil, kapton foil, air, monitor chambers on proton beam trajectory modifies this energy spectrum. The energy distribution at the entrance of the water phantom calculated with an F1 tally for MCNPX using the LA150H library presents a FWHM of 0.5 MeV, as well as a mean energy of 62 MeV, in agreement with the value established by range-energy relation applying ICRU report 49.[16] No differences were observed when calculation was performed with PM. The narrow energy band results from a beam production at an energy ad-hoc to ocular melanoma treatment and the choice of a single scattering system for beam flatness property arrangement. Without thick components inside the beam such as a degrader, the absorbed dose in water is a Bragg peak with a thin distal fall-off of 9×10^{-2} cm between 10% and 90% of dose and a small FWHM of 0.32 cm as shown in Fig. 2.

3. Percentage depth-dose profile

At first, the influence of statistic treatment of the energy loss process was examined on percentage depth-dose profile. Two models were analyzed: the CSDA approximation and the Vavilov model. Data simulated with the CSDA approximation were unable to match experimental points. Data calculated with the Vavilov model were naturally close to experiments especially for the peak zone and even though it requires five times more computation time, it has been retained as model for simulations. The MCS physical process that also fits the shape of energy deposition in peak zone could not be checked, as there is no free parameter to amend it.

Experimental Bragg peak obtained with a parallel plate chamber was compared to MCNPX calculations for the two physics options in Fig. 2. Depth dose profiles have been normalised at z_{max} to analyze relative discrepancies between curves. MC values were calculated with a 0.02 cm step. For the LA150H library, simulated and measured data correlate well and the maximum observed gap are less than 1%. This slight difference is comparable to MC value type A uncertainties and is inferior to experimental data type B uncertainties. For PM, a good agreement is observed for protons having a residual range larger than 1.5 cm where simulated data

present a systematic over-response limited to 1%. This trend was not confirmed for residual range smaller than 1.5 cm. MC values show a significant under-response from 3% to 5%, causing a thinner peak than that described by experimental data. Finally for PM, a 10^{-2} cm deeper penetration not visible on the drawing is observed.

4. Lateral dose profile

Lateral dose profiles were calculated for 1 and 2.5 cm collimator sizes at the entrance of the water phantom by using the LA150H library. Experimental dose points were measured with SD. MC values were calculated with a cylindrical mesh tally type 3 that scores deposited dose in a ring. In order to obtain equivalent type A uncertainties for each MC value, irregular steps were defined. This explains the increasing spacing for decreasing off-axis values. Comparisons between experimental and calculated data, plotted in Fig. 3, present a good agreement. Deviation from experimental values is less than 1%, except in the shoulders where 2% can be reached. These discrepancies are inferior to experimental determinations of type B uncertainties. All data have been normalized at the central axis. Calculations performed with PM, not plotted in this figure, show the same trend and one can conclude that lateral dose profiles are not sensitive to physics options.

5. Absolute absorbed dose

Absolute absorbed dose values at the entrance of the water phantom expressed in MeV cm^{-3}/primary-proton were calculated with the PM and LA150H proton library physics option and compared to FC and IC values (Table II). In the present context primary-proton for simulations should be read as proton-tracks entering the water phantom [box 3 in Fig. 1(b)]. Experimental dose referred to as IC was obtained by dividing the IC response by the proton number scored in FC; the relatively large type B uncertainty associated with this value was due proton number and dose type B uncertainties addition. Experimental dose referred as FC was determined by the CEMA (converted energy per unit mass) assuming a δ-ray equilibrium. This approximation is valid for a

TABLE II. Doses at plateau entrance in MeV cm^{-3}/primary-proton unit. Absolute doses measured with IC, FC, and MCNPX simulated values in PM and LA150H library physics options are reported for a final collimator diameter size set to 2.5 cm.

	IC measurements	FC measurements	MCNPX PM	MCNPX LA150H
Dose (MeV cm^{-3}/primary-proton)	2.09±0.12	1.95±0.03	1.91±0.02	1.90±0.01

homogeneous tissue like the eye but becomes untrue when inhomogeneous medium is involved.[23] Simulated doses were reported with their type A uncertainties. Point of entrance was preferentially chosen for easiest comparison as the proton beam energy spectrum is narrower and the related stopping power, S/ρ involved less extended for dose calculation. This point is a reference for absolute dose determination of the MC calculation.

MC absorbed doses simulated for PM and LAH150 were, respectively, 2% and 2.5% smaller than FC absorbed dose, i.e., close to being in the interval of confidence of the experimental determination. FC dose determination is simply obtained by product of fluence, ϕ, and (S/ρ). When expressed in MeV cm^{-3}/primary-proton unit, this just becomes (S/ρ) divided by the irradiated area, i.e., a quantity independent of proton number measurement for one collimator size. As MCNPX does not produced δ rays, the dose calculation is also processed in the CEMA approximation. As it uses identical S/ρ values for dose scoring, for example 10.516 MeV cm^2 g^{-1} for a proton beam energy of 62 MeV,[16] it is trivial to find FC close value for a beam poorly contaminated by low-energy protons; it also expresses a correct determination of the irradiated area.

MC absorbed doses simulated for PM and LAH150 were, respectively, 8% and 9% smaller than IC absorbed dose, i.e., outside the interval of confidence of the experimental determination. As IC is regarded as the most reproducible reference dosimeter by the last published protocols[24,25] and other works (Refs. 26 and 27), absolute MC dose validation is finally connected with IC and FC dose accordance.[14,28–32] In the literature, FC differences relative to IC vary from −8% to 2%. FC dose measurements are fluence based and the main

source of uncertainties comes from efficiencies of proton collection and electron repulsion by the guard ring. FC is generally homemade with various designs from one site to another that lead to potential variable responses. The use of different IC dose protocols to compare FC to IC is also a potential source of variation. In units of MeV cm^{-3}/primary-proton, the IC value is dependent on the quality of fluence measurements, i.e., finally to FC measurements. When IC and FC dose measurements agree then IC dose automatically agrees with MC dose since FC and MC doses were close. When IC and FC doses disagree then IC and MC doses also disagree.

As doses IC measured and simulated were 8% distant, depth dose and lateral dose profiles were compared in a relative mode. This led to a better appreciation of their relative differences.

6. Output factor

Characterization of narrow beams[33] requires special efforts since the use of finite size detectors can lead to distortion of the measured dose distribution. When collimator size is inferior to small-volume ionization chamber, available detectors are SD and films. The place of MC in such situation was tested throughout output factors (OF) measurements in the simplified case of an unmodulated beam. OF simulated and measured were compared to study collimator size influence on dose and to appreciate capabilities of the code to reproduce such data. Results presented in Fig. 4 show experimental points obtained by SD measurements correctly reproduced by MCNPX calculations, even for the smallest collimator inducing dose collapse. These last data confirm our beam
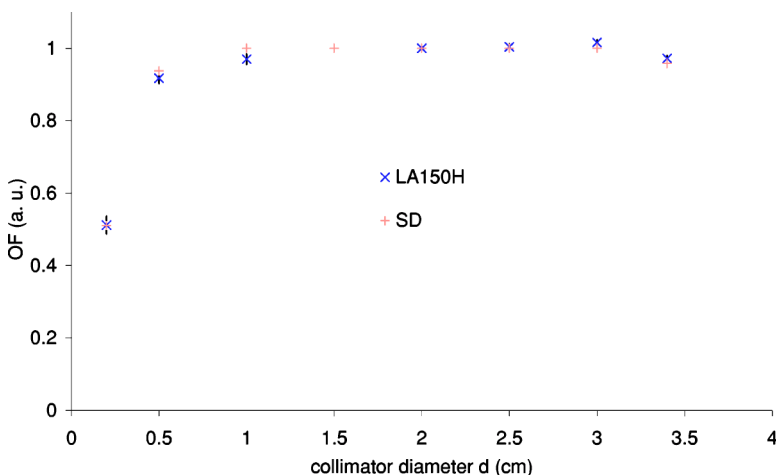

FIG. 4. Output factor, OF, as a function of collimator diameter size, d. OF Bragg peak was determined at the entrance of the water phantom, calculated with MCNPX in LA150H library ($\times$) physics option and measured with SD ($+$). OF normalization is made for 2.5 cm final collimator diameter size. MC type A uncertainties are in the order of 0.5% except for the 0.25 cm collimator presenting 2%. SD type B uncertainties are in the order of 4%.
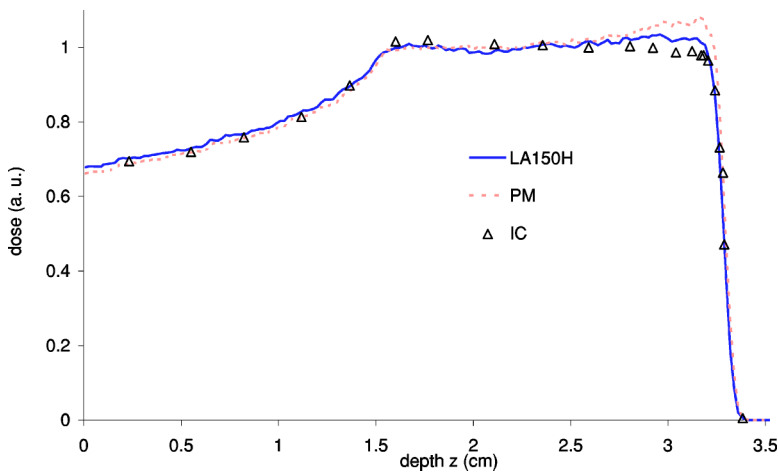
FIG. 5. Relative absorbed dose to water, dose, as a function of water depth, z. SOBP percentage depth-dose, calculated with MCNPX in PM (dashed line) and LA150H library (continuous line) physics options and measured with parallel plate IC (triangle) for a final collimator diameter size set to 2.5 cm. Calculation step size is 0.02 cm. MC type A and parallel plate IC type B uncertainties are, respectively, on the order of 0.5% and 4%.

knowledge more particularly on the slight proton beam divergence leaving OF flat, except for the smallest collimators. These results are coherent with previous measurements made with the help of a Faraday cup (FC).[14] For a collimator diameter wider than twice penumbra, i.e., 0.32 cm, OF is generally admitted as flat, and dose measurements performed for a larger collimator are applied to a smaller one. This assumption is fulfilled except for the 0.5 cm diameter that presents an under-response of 5%. This kind of diameter size can sometimes be reached for clinical irradiation of angioma. IC dose measurements are not performed routinely for collimator size smaller than 1 cm, due to the risk of performing partial irradiation of the chamber volume; only FC measurements heavy to install and relative SD or film measurements are available. In a clinical situation where SOBP is employed, this under-response is more pronounced due to the presence of a Lucite propeller generating lower energy protons. Thus, the MC tool appears as a potential way to define area correction factors, improving absorbed dose determination.

B. Modulated beam

In the MCNPX code geometric entries, there is no way to define a variable thickness of material, as it was needed for Lucite propeller input. So, its description was obtained by a laborious step by step calculation. Sequential addition of reduced weighted Bragg peaks was performed to reproduce the effect of variable range shifting. Weighting factors are those employed to obtain experimentally a flat sum of peaks, i.e., a plateau of peaks homogeneous enough for clinical irradiation. A standard SOPB, used essentially for quality control, was analyzed and compared to PM and LA150H library based calculations. There are more elegant solutions to input propeller[6] when the MC code like GEANT[34] is open to time dependent geometry. The description then becomes more realistic especially for a wheel combining low and high Z materials, which is not the case of our Lucite propeller.

1. Percentage depth-dose profile

Percentage depth-dose profiles from measurements and calculations were plotted in Fig. 5 to study the dependence of the results on physics choice. Experimental data were derived from discrete parallel plate IC dose determinations. MC dose values were calculated each 0.02 cm. Depth dose profiles have been normalised at the middle of the flat part to analyse relative discrepancies between curves.

The PM SOBP shows a slope ending by a bump for the last three peaks exceeding measurements and reaching at its extremity 9%. This disagreement is directly linked to discrepancies noted on a single peak. In fact, when adding the zeroth depth-dose profile D_0 to the first one D_1, which present, respectively, peaks at depths z_{max} and z_{max}^1, the lack of dose upstream z_{max} for D_0 creates a less level summed dose at a depth z_{max}^1 $(D_0(z_{max}^1)+p_1 D_1(z_{max}^1)<D_0(z_{max}))$. The same justification developed for the ith peak leads to a slope shape for the SOBP curve. When observing the decrease of experimental and calculated peak height values in Fig. 6 for the whole reduced contributing Bragg peak D_i, the zeroth, first, and second reduced peaks were over-estimated for the PM physics option, giving in this way for the SOBP a bump above experimental data. Beside distal points, differences between simulated and measured SOBP are found to be smaller than 2%.

The LAH150 SOBP presents a better accordance with experimental data. Excepting the distal 3 mm of the SOBP where discrepancies reach 3%, differences between simulated and measured data are found to be smaller than 2%. These discrepancies are inferior to experimental determinations type B uncertainties. Distal differences are due to a higher gradient variation of peak height (Fig. 6) with Lucite thickness for the three beginning steps of the propeller.

The peak height variation mainly reflects a decrease of proton fluence when material is introduced on beam path. The decrease is mainly due to beam spread out along 2.2 m between box 1 and box 3 that is incidentally caused by MCS.

PM, derived from high-energy physics, exhibits some difficulties in reproducing proximal peak decrease, and the in-
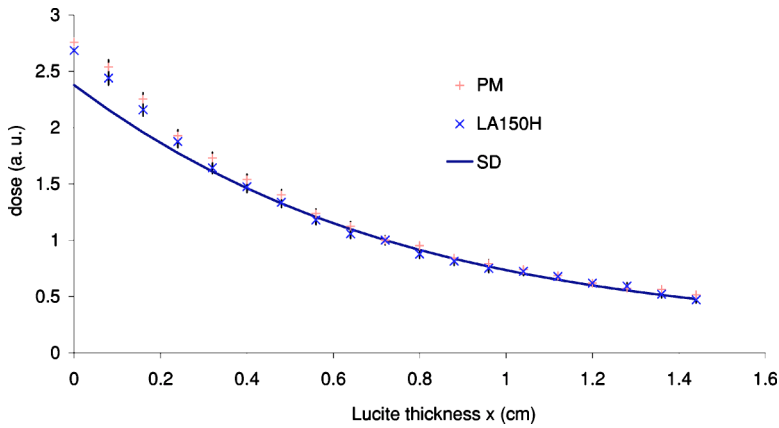
FIG. 6. Unnormalized absorbed dose to water, dose, as a function of incremental Lucite thickness, x. The ordinate represents the height peak of each contributing depth-dose curve $D_i(z)$ obtained by interposition of a Lucite thickness, $x = is$. Value of MCNPX calculations in PM (+) and LA150H library ($\times$) physics options are compared to SD measurements (continuous line). MC type A and SD type B uncertainties are, respectively, on the order of 0.5% and 4%.

accuracy viewed for the single peak is amplified by a cumulative effect. The use of the LA150H library leads to a fair description of clinical SOBP depth-dose profile, presenting no slope and an overestimation of distal dose values smaller than 3%. Analysis of this last series of measurements provides information on an optimal cross-section library choice for the MC calculation with MCNPX, e.g., LAH150.

2. Lateral dose profile

Lateral dose profiles were calculated for 2.5 cm collimator size, both at the entrance of the water phantom and at a depth corresponding to the middle of the plateau of peaks, by using the LA150H library. Experimental dose points were
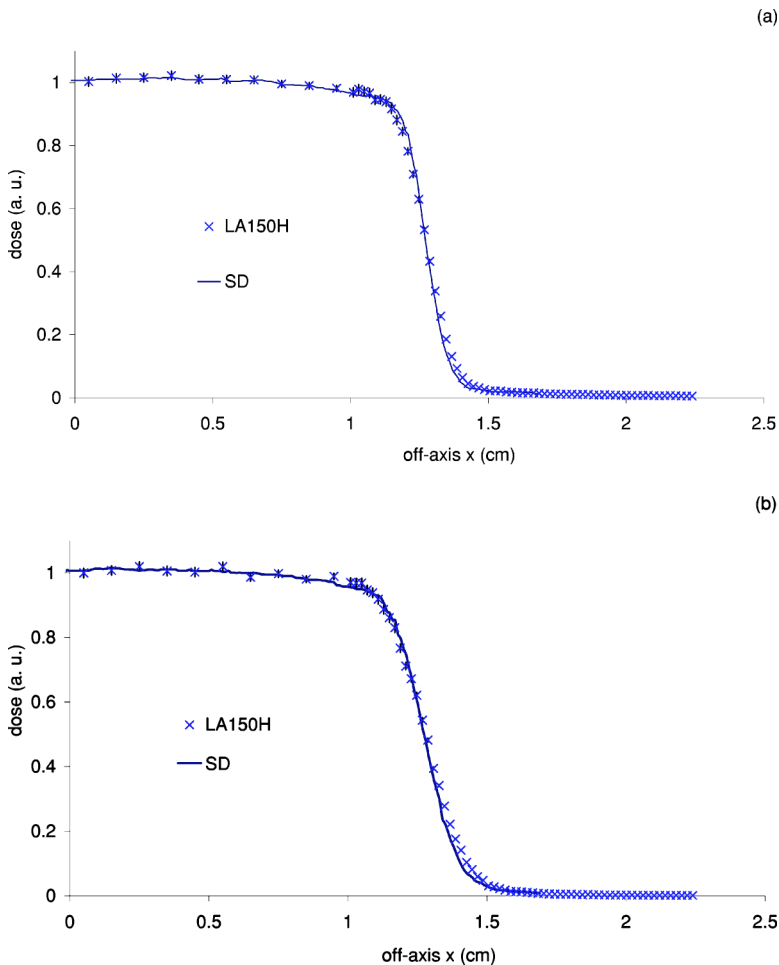
(a)

(b)

FIG. 7. Relative absorbed dose to water, dose, vs lateral position, x. SOBP lateral dose profile calculated with MCNPX in LA150H library ($\times$) physics option and measured with SD (continuous line) at the entrance (a) and in the middle of the plateau of peak (b), for a final collimator diameter size set to 2.5 cm. Calculation step size is irregular; its value is 0.02 cm in the penumbra. MC type A and SD type B uncertainties are, respectively, on the order of 0.5% and 4%.

measured with SD. MC dose points were calculated with irregular steps like for unmodulated lateral dose profiles. All data have been normalized at the central axis. Experimental and calculated data, respectively, plotted for the two depths in Figs. 7(a) and 7(b) correlate well. Deviation from experimental values is less than 2%. Discrepancies are inferior to experimental determinations of type B uncertainties. These results then signify a correct approach to MCS in water, a dense medium in which protons have short range.

IV. UNCERTAINTIES

MC calculation uncertainties are statistical errors and their order of magnitude is strongly linked to the number of protons emitted from the source. It refers only to the precision of the result but not to its accuracy. MC type A uncertainties are typically less than 0.5%, except in peak zone for percentage depth dose profiles and in the central part of lateral dose profiles, where they can reach 1%.

IC uncertainties are mainly due to those found with W_{air}/e one. The European code of practice for proton dosimetry[12,13] concludes to a value of the order of 4%. The Last published IAEA protocol[24] assumes a value of the order of 2% by using a more precisely defined W_{air}/e value. As the European protocol is used in routine and for this study, the first value is retained for type B uncertainties.

FC type B uncertainties[14] are quoted to 1.5% due to uncertainties in beam area and S/ρ values and to the approximation made of an energy spectrum reduced to its modal value.

SD type B uncertainties are quoted in the order of the IC value. This SD was used in routine as relative dosimeter to obtain the shape of the absorbed dose in off-axis or depth. Its response was experienced with various other dosimeters.[35–38] When it was compared to thin detectors avoiding measure convolution, such as a parallel plate chamber, the obtained response was similar. However, SD was recognized to be problematic[39] especially for the *n*-type, due to its dependence to S/ρ values. Additional measurements comparing SD and parallel plate IC were carried out. Results were demonstrated that when unmodulated percentage depth dose was analyzed, SD increases the dose by 3% in the Bragg peak relative to the plateau entrance. For SOBP, 3% were also found between the middle of the flat part and the entrance. SD and IC lateral dose profiles were not subject to variation, as S/ρ remains constant. These discrepancies convenient for routine are problematic for precise comparisons. This explains the use of parallel plate chamber as reference dose detector for the percentage depth dose analysis.

V. CONCLUSION

The presented series of measurements and simulations demonstrate that, with an appropriate choice of beam physics option, MCNPX can be a valuable tool to predict dose, adapted to proton accuracy. In the eye treatment energy range, it involves use of the LA150H library, with Vavilov energy straggling calculation. In this frame, the range and the

dose deposition are correctly described by MC simulation. Dose calculations performed at the entrance of the water phantom show also that absolute determination is available when primary-proton is interpreted as proton tracks entering. However, problems encountered for beam transmission show that MCS must be improved to gain more confidence with MCNPX. The implementation of the full Molière's theory as well as option to turn off MCS is highly desired. Furthermore, access to time-dependant geometry will interest the protontherapy to describe moving mechanical devices. Additionally in a wider interest, secondary electrons production will permit calculations that are more relevant. The CEMA approximation is correct for the eye tissue that presents a homogeneous density. However, it becomes untrue for contiguous inhomogeneous tissues especially near air cavity.

Studies are under way to improve ocular nozzle design for changing its geometric parameters such as collimator size and position or to optimise diffusion devices. However, results have to be taken with caution if MCS plays a significant role, especially for long proton trajectories behind the diffusion point. Another set of studies has also begun, concerning beam modifying-devices that shape the beam, attached to the final patient collimator. In the presence of wedge filters or semi-spherical compensators used to treat conjunctival melanoma,[40,41] the MC technique can accurately calculate proton energy loss and scattering and can aid a better understanding of dose distributions analysis.

ACKNOWLEDGMENTS

a)Electronic mail: joel.herault@nice.fnclcc.fr

[1] A. Courdi, J. P. Caujolle, J. D. Grange, L. Diallo-Rosier, J. Sahel, F. Bacin, C. Zur, P. Gastaud, N. Iborra-Brassart, J. Hérault, and P. Chauvel, "Results of proton therapy of uveal melanomas treated in Nice," Int. J. Radiat. Oncol., Biol., Phys. **45**, 5–11 (1999).

[2] L. Kodjikian, P. Roy, F. Rouberol, J. G. Garweg, P. Chauvel, L. Manon, B. Jean-Louis, R. E. Little, A. J. Sasco, and J. D. Grange, "Survival after proton-beam irradiation of uveal melanomas," Am. J. Ophthalmol. **137**, 1002–1010 (2004).

[3] J. Gambrelle, L. Kodjikian, F. Rouberol, D. Donate, N. Duquesne, B. Jean-Louis, P. Chauvel, J. P. Gérard, P. Romestaing, and J. D. Grange, "Ciliary body melanomas. Survival and prognostic aspects after brachytherapy or proton therapy," J. Fr. Ophtalmol **27**, 40–47 (2004).

[4] Los Alamos National Laboratory, "MCNPX user's Manual Version 2.4.0," LANL Report LA-CP-02-408, 2002.

[5] F. Verhaegen and J. Seuntjens, "Monte Carlo modelling of external radiotherapy photon beams," Phys. Med. Biol. **48**, R107–64 (Review) (2003).

[6] H. Paganetti, "Four-dimensional Monte Carlo simulation of time-dependent geometries," Phys. Med. Biol. **49**, N75–81 (2004).

[7] H. Paganetti, H. Jiang, S. Y. Lee, and H. M. Kooy, "Accurate Monte Carlo simulations for nozzle design, commissioning and quality assurance for a proton radiation therapy facility," Med. Phys. **31**, 2107–2118 (2004).

[8] J. Flanz and H. Paganetti, "Monte Carlo calculations in support of the commissioning of the Northeast Proton Therapy Center," Australas. Phys. Eng. Sci. Med. **26**, 156–161 (2003).

[9] P. Mandrillon, F. Farley, N. Brassart, J. Hérault, A. Susini, and R. Ostojic,

"Commissioning and implementation of the MEDICYC cyclotron programme," XII International Conference on Cyclotron and Their Applications, Berlin, May 1989.

[10] P. Mandrillon, N. Brassart, A. Courdi, P. Chauvel, F. Farley, N. Fétier, J. Hérault, and J. Y. Tang, "Recent activities of the cyclotron laboratory in Nice," XIII International Conference on Cyclotron and their Applications, Vancouver, July 1992.

[11] A. Courdi, N. Brassart, J. Hérault, and P. Chauvel, "The depth-dependent radiation response of human melanoma cells exposed to 65 MeV protons," Br. J. Radiol. **67**, 800–804 (1994).

[12] S. Vynckier, D. E. Bonnet, and D. T. L. Jones, "Code of practice for clinical proton dosimetry," Radiology **20**, 53–63 (1991).

[13] S. Vynckier, D. E. Bonnet, and D. T. L. Jones, "Supplement to the code of practice for clinical proton dosimetry," Radiother. Oncol. **32**, 174–179 (1994).

[14] R. Cambria, J. Hérault, N. Brassart, M. Silari, and P. Chauvel, "Proton beam dosimetry: A comparison between the Faraday cup and an ionization chamber," Phys. Med. Biol. **42**, 1185–1196 (1997).

[15] R. E. Prael and H. Lichtenstein, Los Alamos National Laboratory, "User Guide to LCS: The LAHET Code System," LANL Report LA-UR-89-3014, 1989.

[16] International Commission on Radiation and Units, "Stopping powers and ranges for protons and alpha particles," ICRU Report No. 49, Bethesda, 1993.

[17] P. V. Vavilov, "Ionisation losses of high energy heavy particles," Sov. Phys. JETP **5**, 749–751 (1957).

[18] K. L. Brown, D. C. Carey, C. H. Iselin, F. Rothacker, and European Organization for Nuclear Research, "TRANSPORT, a computer program for designing charged particle beam transport systems," Report CERN 73-16, 1973 & CERN 80-04, 1980.

[19] R. Anne, J. Hérault, R. Bimbot, H. Gauvin, G. Bastin, and F. Hubert, "Multiple angular scattering of heavy ions $^{16-17}$O, ^{40}Ar, ^{86}Kr, ^{100}Mo ions at intermediate energies (20–90 MeV/u)," Nucl. Instrum. Methods Phys. Res. B **34**, 295–308 (1988).

[20] J. Hérault, Institut de Physique nucléaire d'Orsay, "Etude expérimentale du ralentissement d'ions lourds de 20 à 100 MeV par nucléon dans la matière," Report IPNO-DRE-88-25, Orsay, 1988.

[21] W. T. Scott, "The theory of small-angle multiple scattering of fast charged particles," Rev. Mod. Phys. **35**, 231–313 (1963).

[22] K. R. Russell, E. Grusell, and A. Montelius, "Dose calculations in proton beams: Range straggling corrections and energy scaling," Phys. Med. Biol. **40**, 1031–1043 (1995).

[23] F. Verhaegen and H. Palmans, "A systematic Monte Carlo study of secondary electron fluence perturbation in clinical proton beams (70–250 MeV) for cylindrical and spherical ion chambers," Med. Phys. **28**, 2088–2095 (2001).

[24] International Commission on Radiation and Units, "Clinical proton dosimetry. Beam production, beam delivery and measurements of absorbed dose," ICRU Report No. 59, Bethesda, 1998.

[25] International Atomic Energy Agency, *Absorbed Dose Determination in External Beam Radiotherapy: An International Code of Practice for Dosimetry based on Standards of Absorbed Dose to Water*, Technical Report Series No. 398 (IAEA, Vienna, 2001).

[26] J. Medin and P. Andreo, "Monte Carlo calculated stopping-power ratios, water/air, for clinical proton dosimetry (50–250 MeV)," Phys. Med. Biol. **42**, 89–105 (1997).

[27] J. Medin, P. Andreo, and S. Vynckier, "Comparison of dosimetry recommendations for clinical proton beams," Phys. Med. Biol. **45**, 3195–211 (2000).

[28] A. Kacperek and D. E. Bonnet, "Development of a Faraday cup for proton beam dosimetry at the MRC cyclotron unit at Clatterbridge hospital," Proceedings International Heavy Particle Therapy Workshop, 53–6, PSI Villigen, September 1989.

[29] C. S. Mayo, M. Wagner, B. Gottshalk, J. M. Sisterson, and A. Khoeler, "Faraday cup dosimetry in proton beam therapy," Med. Phys. **18**, 625 (abstract) (1991).

[30] E. Grusell, U. Isacsson, A. Montelius, and J. Medin, "Faraday cup dosimetry in a proton therapy beam without collimation," Phys. Med. Biol. **40**, 1831–1841 (1995).

[31] W. D. Newhauser, K. D. Myers, S. J. Rosenthal, and A. R. Smith, "Proton beam dosimetry for radiosurgery: Implementation of the ICRU Report 59 at the Harvard Cyclotron Laboratory," Phys. Med. Biol. **47**, 1369–1389 (2002).

[32] W. D. Newhauser, J. Burns, and A. R. Smith, "Dosimetry for ocular proton beam therapy at the Harvard Cyclotron Laboratory based on the ICRU Report 59," Med. Phys. **29**, 1953–1961 (2002).

[33] S. M. Vatnitsky, D. W. Miller, M. F. Moyers, R. P. Levy, R. W. Schulte, J. D. Slater, and J. M. Slater, "Dosimetry techniques for narrow proton beam radiosurgery," Phys. Med. Biol. **44**, 2789–2801 (1999).

[34] GEANT4, CERN "Toolkit for the simulation of the passage of particles through matter," CERN- Information Technology Division, http://cern.ch/geant4, 1998.

[35] N. Brassart, M. Heintz, J. Hérault, D. Flühs, U. Quast, J. M. Gabillat, W. Sauerwein, and P. Chauvel, "Comparison of different detectors for the determination of Bragg peak," XXth PTCOG Meeting, http://ptcog.mgh.harvard.edu/, Chester, May 1994.

[36] N. Iborra-Brassart, M. Heintz, J. Hérault, D. Flühs, W. Sauerwein, and P. Chauvel, "Comparison of different detectors for the determination of Bragg peak," IAEA RCM: Applications of heavy charged particles in cancer radiotherapy, Vienna, October 1995.

[37] H. Bichsel, "Calculated Bragg curves for ionization chambers of different shapes," Med. Phys. **22**, 1721–1726 (1995).

[38] P. N. Mobit, G. A. Sandison, and C. Bloch, "Depth ionization curves for an unmodulated proton beam measured with different ionization chambers," Med. Phys. **27**, 2780–2787 (2000).

[39] E. Grusell and J. Medin, "General characteristics of the use of silicon diode detectors for clinical dosimetry in proton beams," Phys. Med. Biol. **45**, 2573–2582 (2000).

[40] N. Iborra, J. Hérault, P. Chauvel, and A. Courdi, "Conjunctival melanoma treatment: Physical characteristics of semi-spherical Lucite compensator," 40th PTCOG Meeting, Paris, June 2004.

[41] P. Chauvel, N. Iborra, J. Hérault, A. Courdi, J. P. Caujolle, W. Sauerwein, C. Mosci, S. Squarcia, and J. D. Grange, "Technical requirements, indications and results of protontherapy for conjunctival melanomas," 40th PTCOG Meeting, Paris, June 2004.